Journal of Thermal Analysis and Calorimetry (2024) 149:8041–8057
https://doi.org/10.1007/s10973-024-13245-x

Enhancement of the properties of biodegradable poly(L-lactide)/poly(butylene carbonate) blends by introducing stereocomplex polylactide crystals

Hongda Cheng[1] · Mengdie Yu[2] · Ye Zhang[2] · Hechang Shi[2] · Yancun Yu[2] · Lijuan Wang[1] · Changyu Han[2]

Received: 28 December 2023 / Accepted: 20 April 2024 / Published online: 20 May 2024

Abstract
A low-temperature melt blending method was adopted to prepare ternary blends of poly(L-lactide) (PLLA), poly(butylene carbonate) (PBC), and poly(D-lactide) (PDLA), aiming to obtain fully biodegradable blends with well-balanced properties. The in situ formation of stereocomplex polylactide (SC-PLA) crystals was confirmed by torque changes, differential scanning calorimetry results, and wide-angle X-ray diffraction measurements. At a PDLA concentration of 5 mass%, SC-PLA crystals formed a percolating network structure, and the rheological behavior of the blend melts transformed from liquid-like to solid-like. The viscosity ratio between PLLA and PBC melts increased due to the presence of SC-PLA crystals, resulting in an enlargement of the PBC domain size. SC-PLA crystals exhibited an excellent nucleation effect, significantly accelerating the crystallization rate of PLLA. Compared to neat PLLA with elongation at break of 5.2%, PLLA/PBC/PDLA ternary blends containing 2 mass% PDLA with elongation at break of 247.2% presented excellent toughness. This work provided a facile method to prepare PLLA-based material with outstanding crystallization ability and tailored rheological behavior as well as mechanical properties, which had the potential to replace conventional plastic products.

Keywords Poly(L-lactide) · Poly(butylene carbonate) · Crystallization · Blend · Stereocomplex

Introduction

Petroleum-based plastics have been used extensively in various fields because of their low cost and excellent properties. However, the environmental persistence of these plastics poses a huge challenge to society [1]. Poly(L-lactide) (PLLA) is recognized as a highly promising substitute for petroleum-based plastics since it can be derived from biorenewable resources and exhibits high strength, excellent transparency, and biodegradability [2, 3]. Thus, PLLA has been extensively applied in many fields, such as biomedicine [4], fibers [5], foams [6], agricultural film [7], disposable packaging [8, 9], and 3D printing [10]. Despite displaying many outstanding advantages, PLLA also suffers from serious shortcomings, including high brittleness, slow crystallization rate, and low melt strength, all of which restrict its usage in various applications [11–14]. Many methods, such as plasticization, co-polymerization, and melt blending, have been utilized to toughen PLLA.

Among these methods, melt blending has been confirmed as one of the most efficient approaches to toughen PLLA. In particular, blending PLLA with other biodegradable polymers can enhance the toughness of PLLA while preserving its biodegradability. Currently, various biodegradable polymers, such as poly(butylene adipate-co-terephthalate) (PBAT) [15, 16], poly(ε-caprolactone) (PCL) [17, 18], poly(butylene succinate) (PBS) [19, 20], polyhydroxyalkanoate (PHA) [21], and poly(butylene carbonate) (PBC) [22], have been used as toughening agents of PLLA, with some of them used in conjunction with compatibilizers. However, enhancing the toughness of PLLA and simultaneously increasing its crystallization rate and melt strength remains a challenge for expanding PLLA applications. PBC

✉ Lijuan Wang
wanglj15@ccut.edu.cn

✉ Changyu Han
cyhan@ciac.ac.cn

[1] School of Chemical Engineering, Changchun University of Technology, Changchun 130012, China

[2] Key Laboratory of Polymer Ecomaterials, Changchun Institute of Applied Chemistry, Chinese Academy of Sciences, Changchun 130022, China

is an aliphatic polycarbonate with biodegradability. This polymer can be prepared by transesterification between dimethyl carbonate and 1,4-butanediol in the existence of a heterogeneous catalyst or by polycondensation of PBC oligomer, and 1,4-butanediol, di(4-hydroxybutyl) carbonate, and CO_2 are its final degradation products [23]. Wang et al. [22] prepared PLLA/PBC blends by melt blending method. Their findings indicated that flexible PBC significantly improved the toughness of PLLA, as evidenced by the impact strength and elongation at break of PLLA/PBC blends containing 30 mass% PBC being 25.1 kJ m^{-2} and 299.3%, respectively. Ge et al. [24] investigated the impact of annealing on the mechanical properties of PLLA/PBC blends. They found that prolonged annealing time decreased the toughness of PLLA/PBC blends and enhanced the degree of phase separation.

Adding nucleating agents is considered an effective and reliable approach for enhancing the crystallization ability of PLLA. The use of many inorganic and organic compounds, such as talc [25], layered silicate [26], basalt fibers [27, 28], succinate diphenyl dihydrazide [29], phthalimide [30], and poly(D-lactide) (PDLA) [31], could provide nuclei for PLLA and accelerate the crystallization rate of PLLA. In particular, PLLA and PDLA co-crystallized to form stereocomplex polylactide (SC-PLA) crystals that allow PLLA to crystallize at higher temperatures in non-isothermal crystallization and exhibit fast crystallization kinetics in isothermal crystallization [32]. PDLA also acted as a rheology modifier to enhance the melt strength of the PLLA [33]. Yan et al. [34] investigated the influences of the molecular weight of PDLA (1.5×10^3–18.7×10^3 g mol^{-1}) on the crystallization and rheological behavior of PLLA/PDLA (95/5) blends. Their observations showed that PDLA with too high or too low molecular weight was adverse to form SC-PLA crystals, and PLLA/PDLA blends containing PDLA with a molecular weight of 5.4×10^3 g mol^{-1} exhibited the strongest solid-like viscoelastic behavior and fastest crystallization rate among all prepared samples. Furthermore, formed SC-PLA crystals can impact the mechanical properties of PLLA. Park et al. [35] observed that the formation of SC-PLA crystals increased the mechanical strength of PLLA/PDLA blends. Su et al. [36] found that the elastic modulus and tensile strength of PLLA/PDLA blends increased from 1.13 GPa and 52.98 MPa to 2.04 GPa and 83.70 MPa, respectively, when PDLA content was increased from 0 to 50 mass%.

In this study, we fabricated fully biodegradable PLLA/PBC/PDLA blends with the intention of promoting the crystallization rate, rheological behavior, and mechanical properties of PLLA. The preparation of the blends used a low-temperature melt blending method, i.e., the mixing temperature was lower than the melting temperatures of SC-PLA crystals and higher than that of PLLA, PBC, and PDLA. The changes in torque during melt mixing, along with the results of differential scanning calorimetry (DSC) and wide-angle X-ray diffraction (WAXD), demonstrated the in situ formation of SC-PLA crystals. The study systematically investigated the effect of the formation of SC-PLA crystals on the rheological behavior, morphology development, compatibility, crystallization behavior and kinetics, spherulite morphology, and mechanical properties of the PLLA/PBC blends. It is hoped that fully biodegradable PLLA/PBC/PDLA ternary blends with well-balanced properties can have potential application prospects in various fields.

Experimental

Materials

PLLA (4032D) containing a D-isomer content of 2% was purchased from Nature Works LLC (Nebraska, USA). Its weight average molecular weight (M_w) and polydispersity (M_w/M_n) were 2.07×10^5 g mol^{-1} and 1.73, respectively. PBC, whose M_w and M_w/M_n were 1.23×10^5 g mol^{-1} and 1.81, respectively, was supplied by our collaborator (Institute of Chemistry, Chinese Academy of Science). PDLA containing M_w of 1.25×10^5 g mol^{-1} and M_w/M_n of 1.68 was purchased from Total Corbion Company.

Sample preparation

Before melt mixing, PLLA, PDLA, and PBC were vacuum-dried at 80, 80, and 50 °C for 24 h, respectively. PLLA, PBC, and PDLA were melt mixed by a torque rheometer (XSS-300, Shanghai Kechuang Co., Ltd., China). The mixing screw speed and temperature were set as 60 rpm and 180 °C, respectively. After that, the resultant blends were hot-pressed at 180 °C and 10 MPa for 3 min, followed by cold pressing and quenching at room temperature to obtain the sheet specimens of various thicknesses. For comparison, neat PLLA and binary blend comprising PLLA and PBC were carried out in the same treatment to ensure a consistent thermal history with the ternary blends. For all blends, the mass fraction of PBC was fixed at 20 mass% based on the total mass of blends, and the PDLA concentration varied in a range of 0–10 mass% based on the total mass of PLLA and PDLA components. The PLLA/PBC/PDLA blends were designated as PLLA/PBC-X, in which X denoted the mass fraction of the PDLA component in the blends.

Characterization

Rheological measurements

Rheological measurements were taken using a rotating rheometer (TA Series AR2000ex, TA Instrument, USA)

that processed two parallel plates with a diameter of 25 mm to investigate the rheological behavior of the sample melts. Frequency sweeps ranging from 0.05 to 100 rad s^{-1} at 1.25 strain were performed on the disk samples at 175 °C.

Wide-angle X-ray diffraction (WAXD)

The WAXD measurements were taken on a D8 advance X-ray diffractometer (Bruker, Germany) equipped with a Cu Kα radiation source ($\lambda = 0.154$ nm) at 40 mA and 40 kV. The range of diffraction angle (2θ) covered was 5–40°, with a scanning speed of 3° min^{-1}.

Scanning electron microscopy (SEM)

Cryo-fractured surfaces and impact-fractured surfaces of samples were characterized by SEM (FEI Co., Eindhoven, Netherlands) at acceleration voltages of 5 and 15 kV, respectively. Before observation, the specimens were first crystallized at 100 °C for 1 h, then fractured cryogenically, and finally, surfaces of cryo-fractured specimens were etched using tetrahydrofuran for 40 min at 25 °C. To avoid sample damage, a gold layer was sputtered on the cryo-fractured and impact-fractured surfaces of the samples. The Nano Measurer 1.2 software was used to analyze the distribution and average diameter of the dispersed phase based on SEM images obtained from cryo-fractured surfaces.

Differential scanning calorimetry (DSC)

Thermal analyses were performed using TA Q20 Instruments (USA) under a nitrogen flow of 50 mL min^{-1}. The samples weighing 5–8 mg were placed in aluminum pans. Aiming to evaluate the formation of SC-PLA crystals and matrix crystallinity of mechanical properties testing samples, melt-quenched samples were heated from 0 to 250 °C at 10 °C min^{-1}. For non-isothermal crystallization, each sample was heated from 40 to 190 °C at 100 °C min^{-1}, maintained at 190 °C for 2 min to erase the thermal history, and then cooled to 40 °C at 10 °C min^{-1} (the first cooling) to determine values of the crystallization temperature (T_c) and crystallization enthalpy (ΔH_c). Finally, these samples were reheated to 190 °C at the same rate (the second heating), from which the cold crystallization temperature (T_{cc}), melting temperature (T_m), cold crystallization enthalpy (ΔH_{cc}), and melting enthalpy (ΔH_m) were determined. The crystallinity (X_c) of PLLA in the blends is determined according to Eq. (1).

$$X_c = \frac{\Delta H_m - \Delta H_{cc}}{\Delta H_m^0 \alpha} \times 100\% \quad (1)$$

where $\Delta H_m{}^0$ is the enthalpy of fusion for 100% crystalline PLLA, taken as 93 J g^{-1} [37], and α represents the mass fraction of PLLA.

For isothermal crystallization, samples were heated to 190 °C and equilibrated for 2 min. After that, the molten samples were quenched to crystallization temperature (130 °C or 135 °C) at a cooling rate of 45 °C min^{-1} and held at the crystallization temperature until crystallization was complete.

Polarizing optical microscopy (POM)

The spherulite morphology of PLLA in all samples was observed using POM (Leica DM2500P) equipped with a hot stage (Linkam LTS 350). Before observation, each sample was annealed at 190 °C for 3 min. The molten sample was then annealed at 130 °C for 30 min.

Dynamic mechanical analysis (DMA)

The thermomechanical properties of each sample were evaluated using DMA Q800 (TA Instruments, USA) in tensile mode at a frequency of 1 Hz. The sample with the dimensions of 14 mm × 4 mm × 1 mm (length × width × thickness) was swept from − 60 to 140 °C with a heating rate of 3 °C min^{-1}.

Mechanical properties testing

According to the standard GB/T 1040.1–2006, tensile measurements were taken on a tensile tester (WSM-2KN, Changchun Intelligent Instrument and Equipment Co., Ltd., China) at ambient temperature with a crosshead speed of 5 mm min^{-1}. The dumbbell-shaped specimens, prepared from melt-quenched test sheets, had dimensions of 20 mm × 4 mm × 1 mm (length × width × thickness). A minimum of five specimens were measured for each component. The average value of each tensile property was taken and expressed with standard deviation.

According to the ASTM D256, the notched Izod impact strength of neat PLLA and its blends was determined at ambient temperature using an impact tester (XJUD-5.5, Chengde Jinjian Testing Instrument Co., Ltd., China). Melt-quenched sheets were prepared into standard impact test bars with a v-shaped notch. The average result of five tests for each sample was taken and expressed with standard deviation.

Results and discussion

Stereocomplex formation

Figure 1a shows the torque versus time curves for neat PLLA and its blends during melt mixing. The loading

peaks with various heights were observed at the initial stage, ascribed to the feeding and melting of PLLA, PBC, and PDLA pellets. The blends displayed lower loading peaks than neat PLLA owing to the elasticity of PBC at room temperature. A relatively stable plateau was observed with the increase in time, indicating that the torque value reached an equilibrium (balance torque). Incorporating PBC reduced the balance torque of PLLA, which might be because the presence of PBC decreased the interaction between the PLLA chains. The PLLA/PBC/PDLA ternary blends containing 5 and 10 mass% exhibited higher balance torque than the PLLA/PBC binary blend, and the balance torque of PLLA/PBC-10 was higher than that of PLLA/PBC-5. The observed phenomena might be attributed to the co-crystallization of PLLA and PDLA, which formed SC-PLA crystals. These crystals with high modulus as solid particles reinforced the blend melts. Moreover, during melt processing, the co-crystallization of PLLA and PDLA restrained the mobility of PLLA chains, which increased the melt viscosity of blends and resulted in a higher balance torque. If SC-PLA crystals were not formed, the balance torque of ternary blends should decrease with increasing PDLA concentration due to its lower molecular weight than PLLA. However, instead of a decrease, the addition of PDLA significantly increased balance torque. Therefore, it could be verified that adding PDLA in the binary blend formed the SC-PLA crystals. It was noted that the torque curves of the PLLA/PBC-2 sample did not significantly change compared to that of the PLLA/PBC binary blend. This phenomenon might be due to less formation of SC-PLA crystals in blends containing 2 mass% PDLA.

DSC tests of melt-quenched samples further confirmed the in situ formation of SC-PLA crystals. DSC curves of neat PLLA and its blends are shown in Fig. 1b. The samples without PDLA showed only one melting peak at around 170 °C. Ternary blends with various PDLA concentrations displayed two distinct melting peaks, approximately 169 and 221 °C, representing the melting characteristics of homocrystallites and stereocomplex crystals of PLA, consistent with previous reports [38]. Furthermore, ternary blends with higher PDLA concentrations showed a larger exothermic area at around

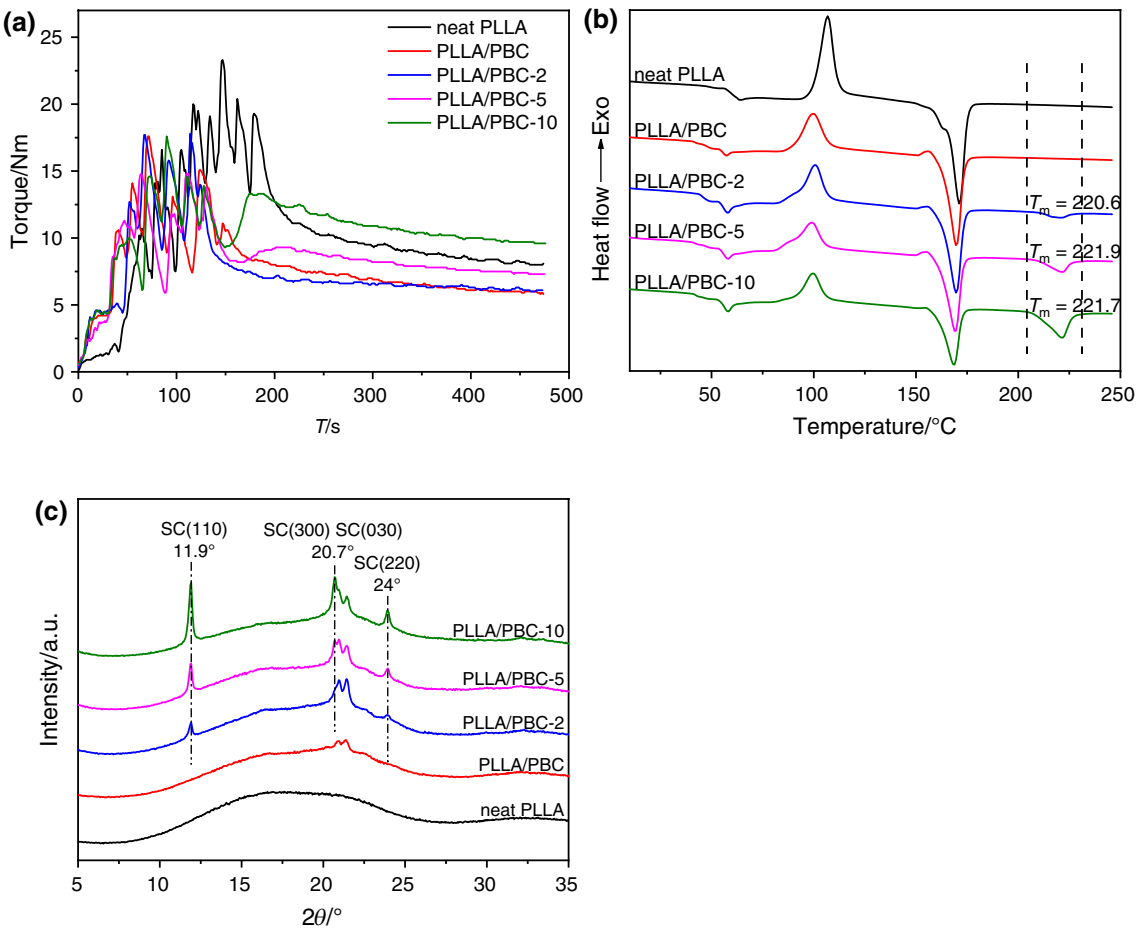

Fig. 1 **a** Torque versus time curves; **b** DSC curves at a heating rate of 10 °C min^{-1}; **c** WAXD patterns of neat PLLA and its blends

221 °C, indicating that more SC-PLA crystals were formed with the increasing PDLA concentration.

WAXD is a direct and effective way to confirm the in situ formation of SC-PLA crystals. Figure 1c shows the WAXD patterns of neat PLLA and its blends. It is clear that no diffraction peaks of PLLA and PDLA homocrystallites at 2θ of 16°, 18.4°, and 21.8° were detected [39]. However, after adding PDLA into PLLA/PBC binary blend, three typical diffraction peaks were observed at 11.9°, 20.7°, and 24°, corresponding to (110), (300)/(030), and (220) planes of SC crystal structure [40]. Furthermore, when PDLA content increased from 2 to 10 mass%, the intensity of these peaks gradually increased, indicating an increase in the formation of SC-PLA crystals, consistent with the DSC results in Fig. 1b.

Rheological behavior

In order to study the influence of SC-PLA crystals on the rheological behavior of PLLA/PBC blend melts, the oscillatory shear rheological test was conducted at 175 °C. Figure 2 illustrates storage modulus (G'), loss modulus (G''), complex viscosity ($|\eta^*|$), and damping factor ($\tan\delta = G''/G'$) as a function of angular frequency for neat PLLA, PLLA/PBC binary, and PLLA/PBC/PDLA ternary blends, respectively.

As seen in Fig. 2a and b, the blends exhibited higher G' and G'' than neat PLLA. The G' and G'' of neat PLLA revealed a good linear relationship with the angular frequency at low frequencies, representing typical liquid-like behavior. The addition of PDLA increased the G' and G'' of the binary blend, and the G' and G'' of ternary blends increased with increasing PDLA concentration. Moreover, the slopes of G' for ternary blends at low frequencies decreased as the PDLA concentration increased. In particular, for the PLLA/PBC-10 sample, the dependence of the slope of G' on angular frequency almost disappeared at low frequencies, implying the pseudo-solid-like behavior of the blend melts. This finding might be due to the formation of a percolating network structure composed of SC-PLA crystals with high modulus, which significantly strengthened the blend melts.

From Fig. 2c, it was distinct that the blends showed higher $|\eta^*|$ than neat PLLA at all frequencies. Neat PLLA exhibited a long Newtonian plateau. However, ternary blends showed

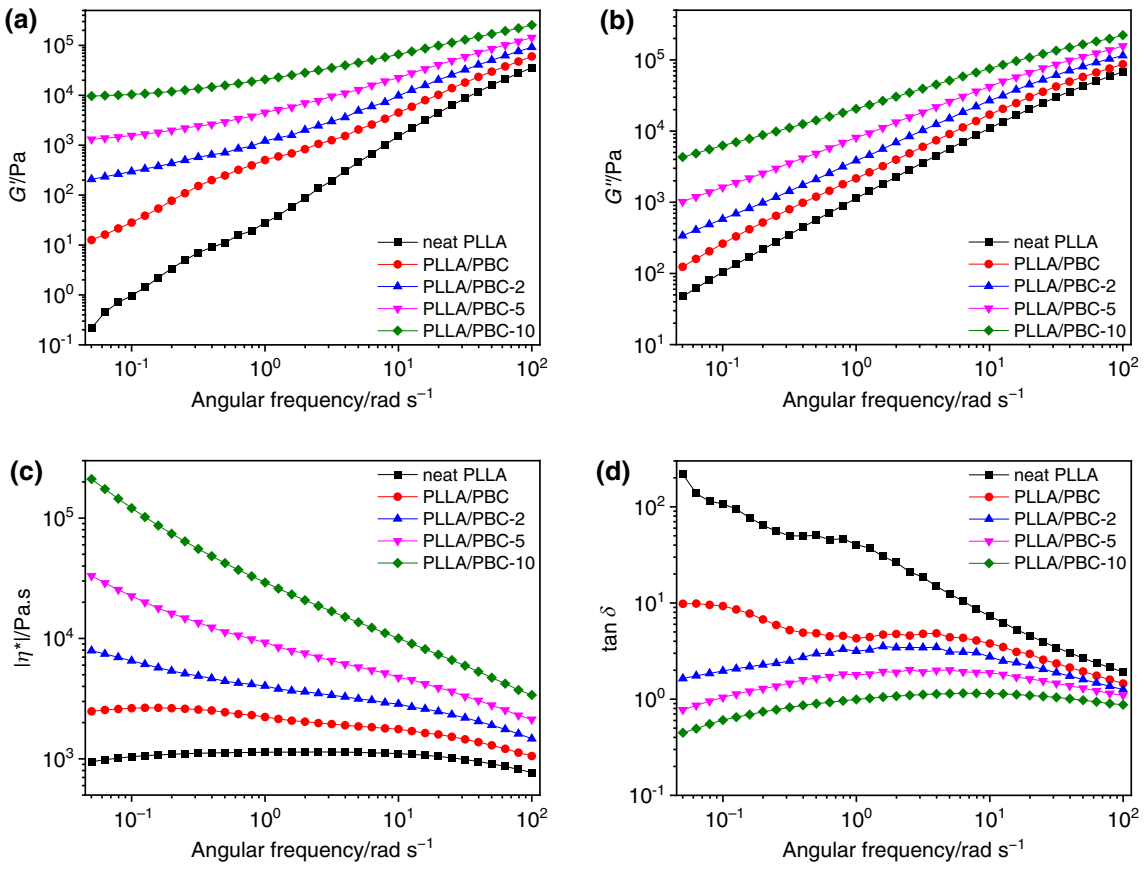

Fig. 2 **a** Storage modulus (G'), **b** loss modulus (G''), **c** complex viscosity ($|\eta^*|$), and **d** damping factor ($\tan\delta$) of neat PLLA and its blends as a function of angular frequency at 175 °C

typical non-Newtonian shear-thinning behavior, implying that SC-PLA crystals could form a percolating network structure. Moreover, $|\eta^*|$ of ternary blends increased as the PDLA concentration increased, suggesting that the existence of SC-PLA crystals improved the melt viscosity of blends.

It could be observed in Fig. 2d that the tan δ of neat PLLA decreased with the increase in angular frequency, suggesting its viscoelastic liquid behavior. The blends presented lower tan δ than neat PLLA at given frequencies. Furthermore, the addition of PDLA reduced tan δ of the binary blend, and tan δ of the ternary blends decreased as the PDLA concentration increased. These phenomena implied that the introduction of SC-PLA crystals promoted the melt elastic response of ternary blends.

Since the modulus is sensitive to SC-PLA crystal network structure, Fig. 3 illustrates the variations of G' and G'' at 0.05 rad s^{-1} with PDLA concentration for all blends. The turning point of plots can serve as a percolation threshold to confirm the formation of the SC-PLA crystal network [41]. It could be observed that the percolation threshold of the SC-PLA crystal network structure formed in blends was a PDLA concentration of 5 mass%. Another piece of evidence is provided in Fig. 4, which compares G' and G'' of blends at all frequencies. For the PLLA/PBC and PLLA/PBC-2, G' was lower than G'' at all frequency ranges, implying that deformation was predominantly viscous. For PLLA/PBC-5, the curves of G' and G'' showed a crossing point at low frequencies, indicating that deformation was predominantly viscoelastic due to the buildup of the SC-PLA crystal network [42]. As the PDLA concentration increased, the crossing point moved to high angular frequencies, such as PLLA/PBC-10, implying a more prominent elastic response.

In general, the investigation of rheological behavior demonstrated that formed SC-PLA crystals with high modulus significantly strengthened the blend melts and increased its elastic response. After adding 5 mass% PDLA into the binary blend, the SC-PLA crystal network structure was formed, causing the rheological behavior of the blend melts to change from liquid-like to solid-like. In addition, attributing strong intermolecular hydrogen bonding interaction, PLLA and PDLA chains were co-crystallized within the stereocomplex, which might markedly restrain the chain motion of the PLLA. The relaxation of chain segments for the PLLA matrix was also restricted.

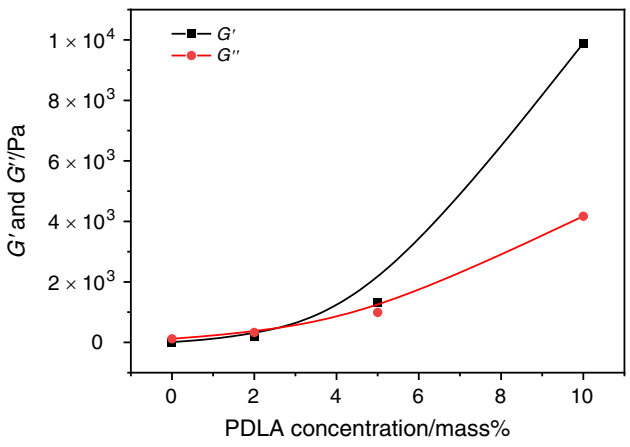

Fig. 3 The relationship between G' and G'' of blends at a frequency of 0.05 rad s^{-1} and the concentration of PDLA

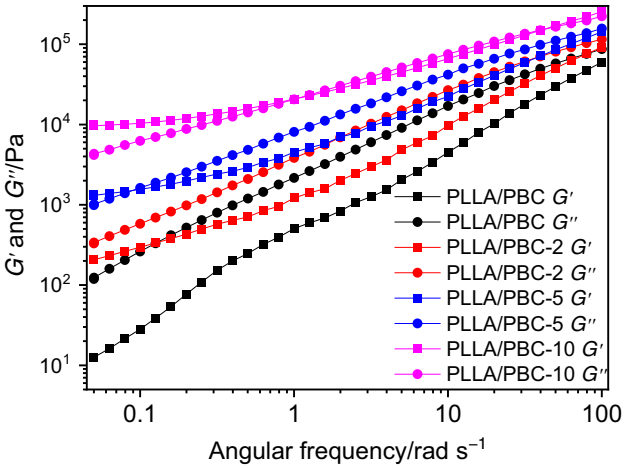

Fig. 4 Plots of G'' and G'' of PLLA/PBC binary and PLLA/PBC/PDLA ternary blends

Phase morphology

In order to reveal the impact of SC-PLA crystals on PBC distribution in the PLLA matrix, the phase morphologies of blends were characterized using SEM. Figure 5 presents the cryo-fractured surfaces of blends after removing the PBC phase. The blends presented typical "sea–island" microphase separation morphology, illustrating that the PBC phase and the PLLA matrix were immiscible. This result was consistent with previous reports [22, 24]. Unexpectedly, the addition of PDLA increased the PBC domain size. The PBC domain size distribution obtained by the Nano Measurer 1.2 software analysis is plotted in Fig. 6. It was found that the average diameter (D) of PBC domains in the PLLA/PBC binary blend was around 1.62 μm. However, with increasing the PDLA concentration, the D value of PBC domains increased to 3.15, 4.29, and 5.21 μm for PLLA/PBC-2, PLLA/PBC-5, and PLLA/PBC-10, respectively. In addition, the structure and shape of the dispersed PBC phase became very complex. Some dispersed PBC domains transformed from spheres to ellipsoids with increasing PDLA concentration. When the PDLA concentration reached 10 mass%, the dispersed PBC phases exhibited irregular shape.

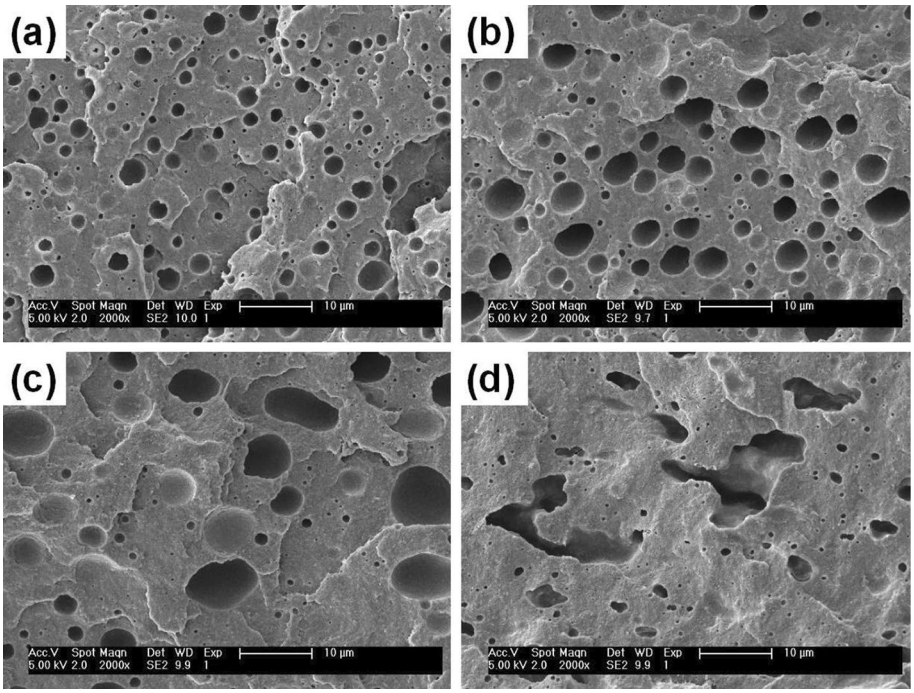

Fig. 5 SEM images of etched PBC phase for blends: **a** PLLA/PBC; **b** PLLA/PBC-2; **c** PLLA/PBC-5; and **d** PLLA/PBC-10

It is well established that the equilibrium between the breakup and coalescence of dispersed droplets is a primary mechanism that governs the morphology evolution for a mount of immiscible polymer pairs. Furthermore, some factors, such as interfacial tension, processing parameters, blend composition, and viscosity ratio, also influenced the final morphology of blends [43]. All blends had the same interfacial tension, processing parameters, and blend composition in this work. Hence, viscosity changes of the PLLA matrix arising from the co-crystallization of PLLA and PDLA might play a critical role in the morphological evolution. For immiscible polymer pairs, there was a mixing degree. When polymer pairs had similar melt viscosities, i.e., viscosity ratio ≈ 1, the finest dispersion could be achieved, where the mixing degree approached molecular mixing [44]. As seen in Fig. 2c, the in situ formation of SC-PLA crystals increased the melt viscosity of the PLLA matrix, which could reduce the mixing degree and thus result in phase coarsening. In particular, when the PDLA concentration reached 5 mass% or more, the blend melts showed solid-like viscoelastic characteristics, which might adversely impact the equilibrium between the breakup and coalescence of the dispersed droplets. In addition, when considering the impact of component elasticity, the dynamic balance between deformation and deformation-resisting forces was an additional critical factor in controlling deformation and the final morphology [45]. The SC-PLA crystal network imposed an impediment effect on the flow of PLLA melt, reducing the transfer of shear stress from the PLLA matrix to the PBC phase, ultimately resulting in detrimental effects on the deformation and breakup of the PBC phase [46]. It has been reported that the high energy input would increase the collision forces of dispersed droplets in the blend melts, causing more coalescence [47]. It can be observed from Fig. 1a, as the increase in PDLA concentration, the balance torque of PLLA/PBC/PDLA ternary blends showed a sharp increase compared to PLLA/PBC binary blend, which inevitably caused high energy input, consequently increasing the number of dispersed droplets collision. Therefore, the introduction of SC-PLA crystals led to larger PBC domain sizes and aspect ratios.

Thermal and crystallization behaviors

The non-isothermal crystallization behavior of each sample was analyzed using DSC curves to investigate the effect of the formation of SC-PLA crystals on the thermal properties of PLLA/PBC/PDLA ternary blends. Figure 7 shows the DSC curves of all samples, and the key thermal parameters are listed in Table 1.

From the first cooling curves shown in Fig. 7a, no exothermic peak was observed for neat PLLA owing to its poor crystallization ability. In contrast, a broad crystallization peak of PLLA appeared at around 109.2 °C for PLLA/PBC-2. This phenomenon also confirmed the formation of SC-PLA crystals, which promoted PLLA crystallization. As the amount of SC-PLA crystals formed increased, the crystallization peak became sharper and shifted to higher temperatures, especially for the PLLA/PBC-10. These findings indicated that the excellent nucleation effect of SC-PLA

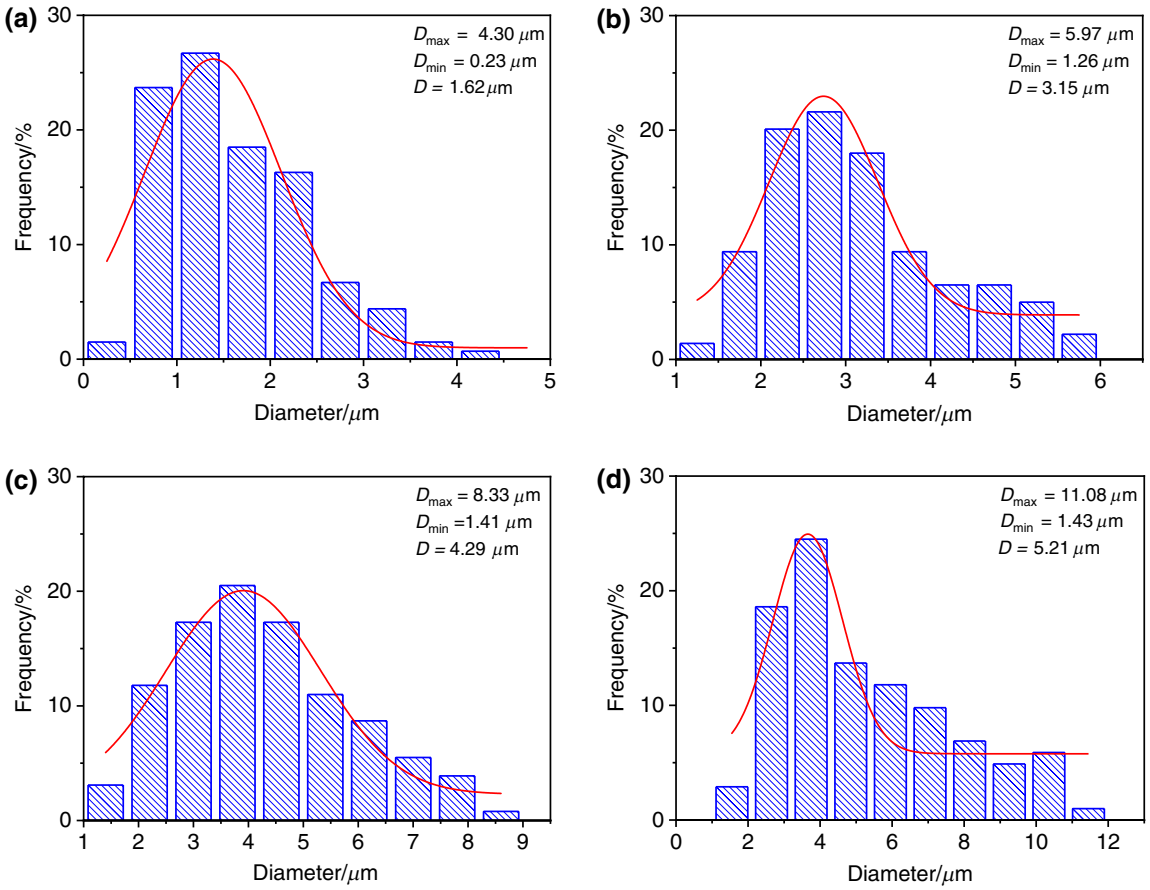

Fig. 6 Size and distribution of dispersed PBC domains as determined from SEM images: **a** PLLA/PBC; **b** PLLA/PBC-2; **c** PLLA/PBC-5; and **d** PLLA/PBC-10. The D_{max}, D_{min}, and D represent the maximum, minimum, and average diameter of the PBC domains

crystals significantly enhanced the melt crystallization ability of PLLA in ternary blends.

In the second heating scans, neat PLLA exhibited cold crystallization and melting behavior at around 103.0 and 169.5 °C, respectively, as shown in Fig. 7b. For the binary blend, adding PBC increased the cold crystallization temperature (T_{cc}) of PLLA, indicating that PBC reduced the cold crystallization ability of PLLA. It is worth noting that the DSC curve of the binary blend presented double melting peaks of PLLA. The low melting peak (T_{m1})

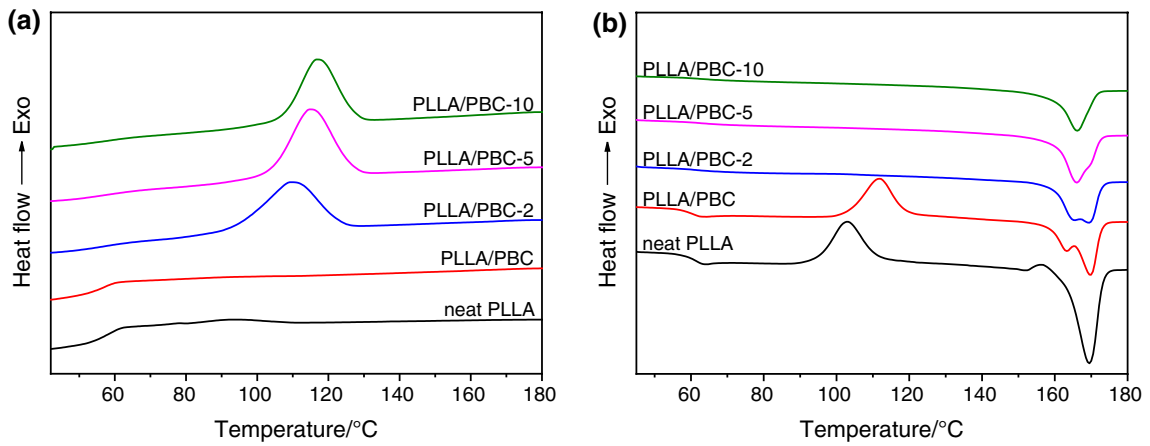

Fig. 7 DSC curves at 10 °C min^{-1} for all samples: **a** first cooling and **b** second heating

Table 1 Thermal parameters obtained from DSC curves for all samples

Sample	First cooling		Second heating					
	T_c/°C	ΔH_c/J g^{-1}	T_{cc}/°C	ΔH_{cc}/J g^{-1}	T_{m1}/°C	T_{m2}/°C	ΔH_m/J g^{-1}	X_c/%
Neat PLLA	–	–	103.0	37.4	–	169.5	43.7	6.8
PLLA/PBC	–	–	111.9	37.3	162.9	169.8	44.1	7.1
PLLA/PBC-2	109.2	34.6	–	–	164.5	169.4	41.7	44.8
PLLA/PBC-5	114.6	39.3	–	–	166.0	–	43.7	47.0
PLLA/PBC-10	116.5	35.5	–	–	166.2	–	35.5	38.2

corresponded to the melting of unstable defective crystals, and the high melting peak (T_{m2}) corresponded to the melting of perfect crystals produced by melting–recrystallization. For PLLA/PBC/PDLA ternary blends, the cold crystallization peak of PLLA disappeared, suggesting that PLLA crystallized completely during the cooling process due to the excellent nucleation effect of SC-PLA crystals. Furthermore, ternary blends also displayed double melting peaks, and the peak of T_{m1} became more intense than that of T_{m2} with increasing PDLA concentration. When the PDLA concentration reached or exceeded 5 mass%, the peak of T_{m2} vanished. These phenomena indicated that the introduction of SC-PLA crystals accelerated the PLLA crystallization rate in ternary blends, thus forming more unstable defective crystals.

From Table 1, the crystallinity (X_c) of neat PLLA was approximately 6.8% and that of the PLLA/PBC binary blend was approximately 7.1%. For PLLA/PBC/PDLA ternary blends, the incorporation of PDLA dramatically increased X_c of PLLA because of the formation of SC-PLA crystals promoting PLLA crystallization by acting as heterogeneous nucleating agents. Moreover, the X_c of PLLA in ternary blends initially increased and then decreased with increasing PDLA concentration. When PDLA concentration reached 5 mass%, the X_c was highest with a value of 47.0%. Therefore, it was essential to discuss how the introduction of PDLA and its concentration variations in the ternary blends impact the crystallization behavior of PLLA. The polymer crystallization is controlled by two independent processes: the initial formation of crystal nuclei and the subsequent growth of the crystals [14]. Initially, as shown in Fig. 7a, SC-PLA crystals significantly enhanced the crystallization ability of PLLA in ternary blends as an effective nucleating agent. Furthermore, during the crystal growth process, PLLA chain segments must overcome the energy barrier to diffuse and adhere to the growing front of the crystals. Apart from acting as nucleating agents, SC-PLA crystals acted as physical crosslinks dispersed in the PLLA matrix, restricting the motion of PLLA chain segments and inhibiting their transport to the growing front of the crystals. Therefore, when PDLA concentration increased to 10 mass%, the positive effects of nucleating agents were overwhelmed by the negative effects of physical crosslinks, ultimately leading to the decrease in X_c.

Isothermal melt crystallization behavior and kinetics

The isothermal melt crystallization behavior of neat PLLA and its blends was also studied by DSC, aiming to reveal further the impact of SC-PLA crystals on the thermal properties of PLLA/PBC/PDLA ternary blends. The testing results are shown in Fig. 8. For PLLA/PBC binary blend, PBC shortened the crystallization time of PLLA to some degree at the same crystallization temperature (T_c). For the immiscible blend system, the acceleration of the crystallization rate might be ascribed to the increased chain segment mobility at the phase interface, which facilitated the formation of nucleation sites [48]. However, the crystallization time of PLLA was significantly reduced after the addition of PDLA.

The equation for determining relative crystallinity (X_t) at time (t) is as follows:

$$X_t = \frac{X_c(t)}{X_c(\infty)} = \int_0^t \frac{dH(t)}{dt}dt \Big/ \int_0^\infty \frac{dH(t)}{dt}dt \quad (2)$$

where $X_c(t)$ and $X_c(\infty)$ denote the crystallinity at time t and the end of time, respectively; $dH(t)/dt$ denotes the heat flow rate [49]. Figure 9 shows the plots of X_t versus t for neat PLLA and its blends at different T_cs. It was evident that raising T_c from 130 to 135 °C extended the crystallization time of PLLA in each sample. This phenomenon was due to the crystallization process needing supercooling. The decrease in supercooling reduced the driving force of crystallization, which made nucleation difficult and resulted in an extension of the crystallization time [50].

The isothermal melt crystallization kinetics of the PLLA component in each sample were analyzed using the Avrami model, expressed by the following Eq. (3) [51, 52]:

$$X_t = 1 - \exp(-kt^n) \quad (3)$$

where k and n represent crystallization rate constant and Avrami exponent, respectively [53]. Based on the fitted straight lines shown in Fig. 10, the k and n values could be determined from the intercept and slope, respectively. The

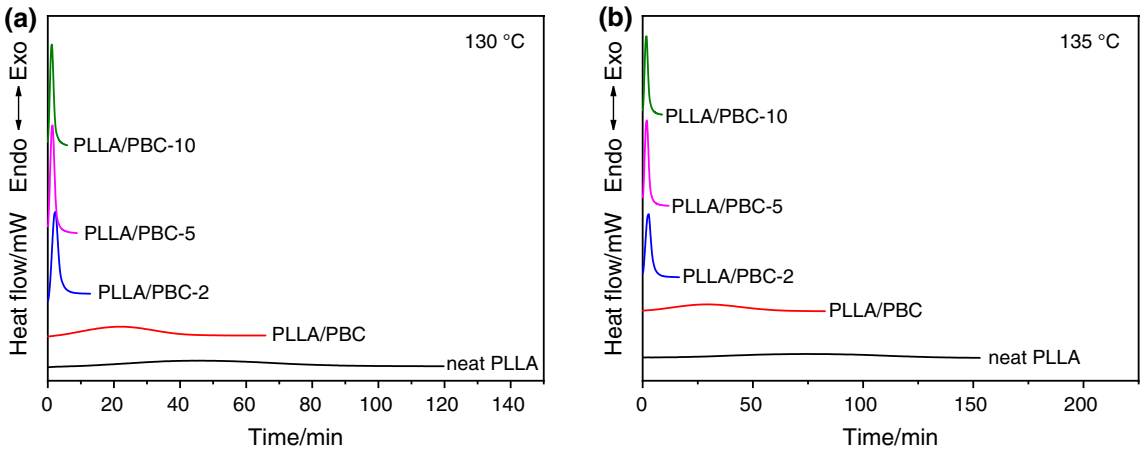

Fig. 8 DSC curves of isothermal crystallization for neat PLLA and its blends at **a** 130 °C and **b** 135 °C

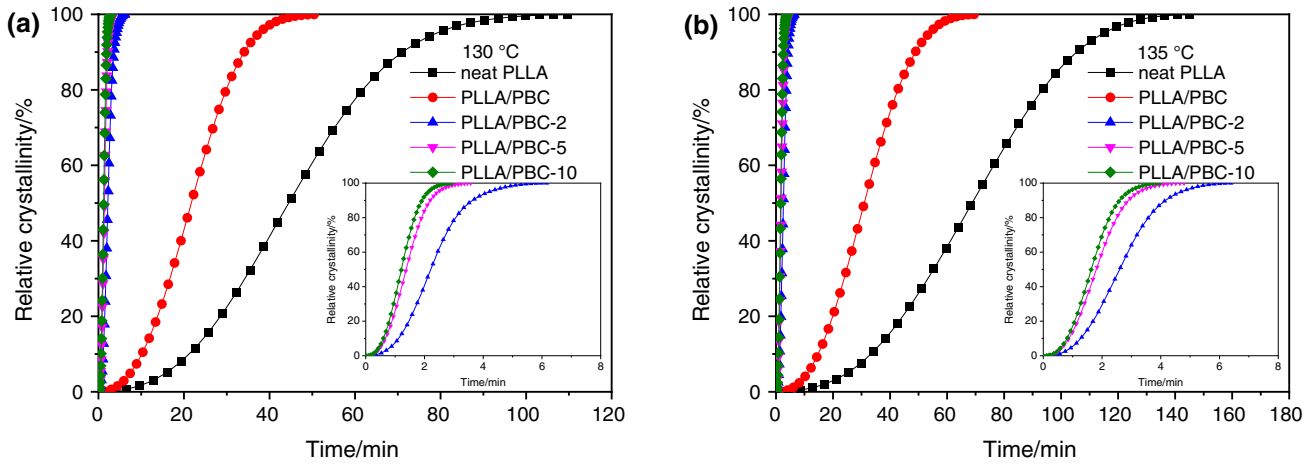

Fig. 9 Plots of relative crystallinity versus time for neat PLLA and its blends at **a** 130 °C and **b** 135 °C

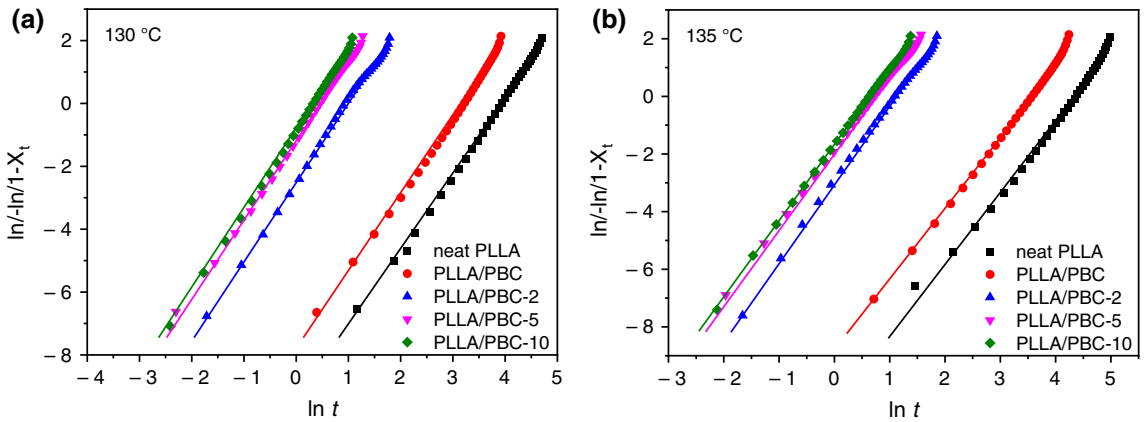

Fig. 10 Avrami plots of isothermal crystallization at **a** 130 °C and **b** 135 °C for neat PLLA and its blends

Table 2 Isothermal melt crystallization kinetic parameters for neat PLLA and its blends based on the Avrami model

Sample	$T_c = 130$ °C				$T_c = 135$ °C			
	$t_{1/2}$/min	n	k/min^{-n}	R^2	$t_{1/2}$/min	n	k/min^{-n}	R^2
Neat PLLA	43.8	2.5	6.11×10^{-5}	0.9986	66.0	2.5	1.80×10^{-5}	0.9917
PLLA/PBC	20.9	2.5	3.71×10^{-4}	0.9972	30.2	2.6	1.13×10^{-4}	0.9975
PLLA/PBC-2	2.31	2.5	0.0843	0.9980	2.6	2.7	0.0519	0.9990
PLLA/PBC-5	1.4	2.5	0.3112	0.9989	1.8	2.5	0.1515	0.9995
PLLA/PBC-10	1.2	2.6	0.4172	0.9996	1.6	2.6	0.1842	0.9995

corresponding kinetics parameters are given in Table 2. The Avrami model was suitable for describing the isothermal melt crystallization kinetics of these blend systems due to the R^2 values of approximately 1. The n values of neat PLLA at different T_cs were close to 2.5, implying that the crystallization mode was homogeneous nucleation with two-dimensional growth [54]. The n values of blends ranged from 2.5 to 2.7, implying that the crystallization mode was instantaneous nucleation with three-dimensional growth [55]. The k values of each sample are also provided in Table 2. Since the unit of k was min^{-n}, in which the n value varied with PDLA concentration, it is hard to accurately compare and evaluate the isothermal melt crystallization rate using the k value. Therefore, the crystallization half-time ($t_{1/2}$), the time taken from the onset of crystallization to the point at which X_t reaches 50%, is an essential parameter for evaluating the isothermal melt crystallization rate. It can be calculated using the following Eq. (4):

$$t_{1/2} = \left(\frac{\ln 2}{k}\right)^{1/n} \tag{4}$$

The obtained results are shown in Table 2. The PLLA/PBC binary blend exhibited a smaller $t_{1/2}$ value at the same T_c than neat PLLA. The introduction of PDLA sharply reduced the $t_{1/2}$ of PLLA in blends. For instance, at a T_c of 135 °C, the $t_{1/2}$ of neat PLLA was approximately 66.0 min, but the $t_{1/2}$ of PLLA/PBC-2 decreased to approximately 2.6 min, a decrease of approximately 24 times. In addition, the reducing trend of $t_{1/2}$ became slower with increasing PDLA concentration. All of these observations again indicated that SC-PLA crystals were an effective nucleating agent that significantly accelerated the crystallization rate of PLLA.

Spherulite morphology

To explore the impact of SC-PLA crystals on the spherulite morphology of PLLA in PLLA/PBC/PDLA ternary blends, PLLA spherulites grown at 130 °C for 30 min after cooling from 190 °C were observed utilizing POM. Figure 11 presents the images of PLLA spherulites in each sample. Neat PLLA exhibited some large-sized spherulites with a diameter of about 100 μm, as seen in Fig. 11 (a). Compared to neat PLLA, incorporating PBC increased nucleation density and decreased PLLA spherulite size, as evidenced by Fig. 11b. POM images of ternary blends with PDLA concentration increased from 2 to 10 mass% are presented in Fig. 11c–e. It was not easy to distinguish individual spherulites upon incorporating PDLA. This finding was attributed to the fact that SC-PLA crystals acted as a heterogeneous nucleating agent, which significantly increased the density of crystal nuclei, resulting in spherulites impinging with surrounding spherulites during the growth process, thereby inhibiting their further growth.

Dynamic mechanical analysis

The effect of introducing SC-PLA crystals on the thermo-mechanical properties of the PLLA/PBC binary blend was investigated using DMA. Figure 12a and b presents DMA traces of damping factor (tan δ) and storage modulus (E') versus temperature for neat components and their blends, respectively.

The appearing peak on tan δ curves represents the glass transition temperature (T_g) and the molecular chain mobility transition. Neat PBC and PLLA exhibited a T_g at about − 21.6 and 60.7 °C, respectively. PLLA/PBC binary blend displayed two damping peaks at around − 28.3 (T_g for PBC) and 60.2 °C (T_g for PLLA), demonstrating that PLLA and PBC were immiscible, consistent with the SEM results and previous reports [22]. It is worth noting that the T_g of PBC blended with PLLA showed a decrease of around 7 °C compared to that of neat PBC, which could be due to the existence of the phase interface between the PLLA matrix and PBC phase. Enrichment of short chains, small molecules, and chain end groups at the phase interface of immiscible blends would increase chain mobility because of excess free volume, which could result in a depression of T_g of the dispersed phase [48]. In addition, the T_g values of PLLA and PBC components in the PLLA/PBC/PDLA ternary blends had almost no change as PDLA concentration increased, implying that the addition of PDLA had little influence on the miscibility of PBC and PLLA.

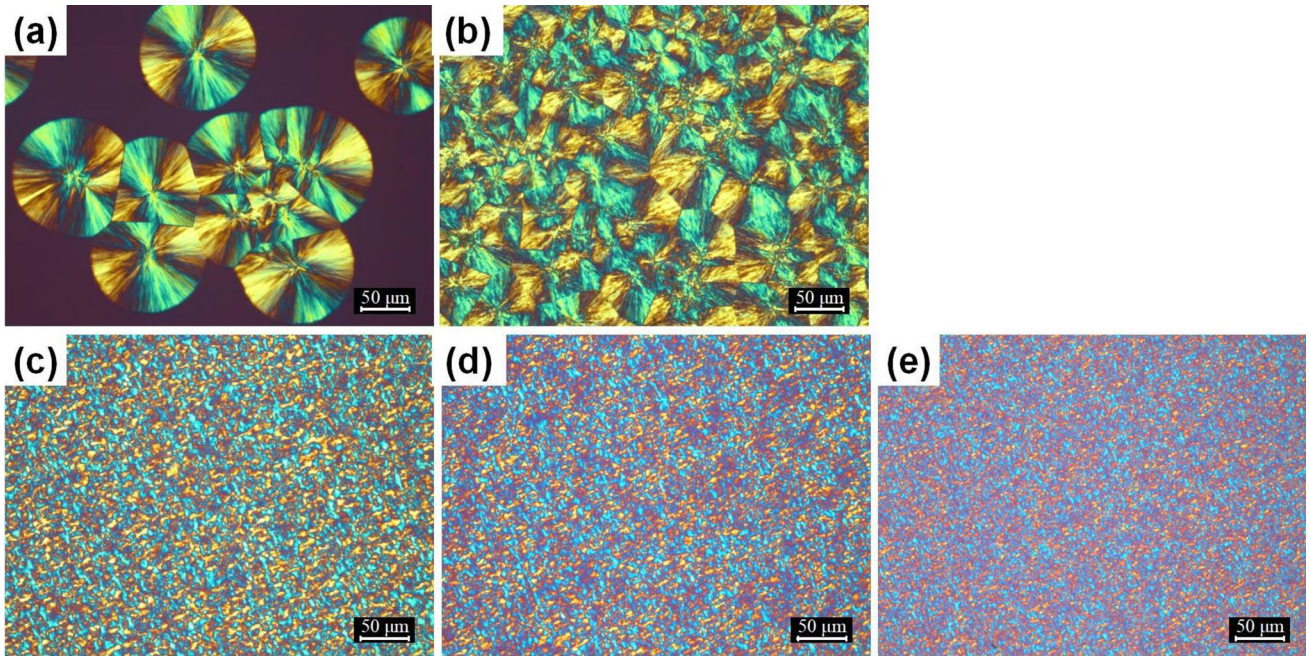

Fig. 11 Spherulite morphology: **a** neat PLLA; **b** PLLA/PBC; **c** PLLA/PBC-2; **d** PLLA/PBC-5; and **e** PLLA/PBC-10

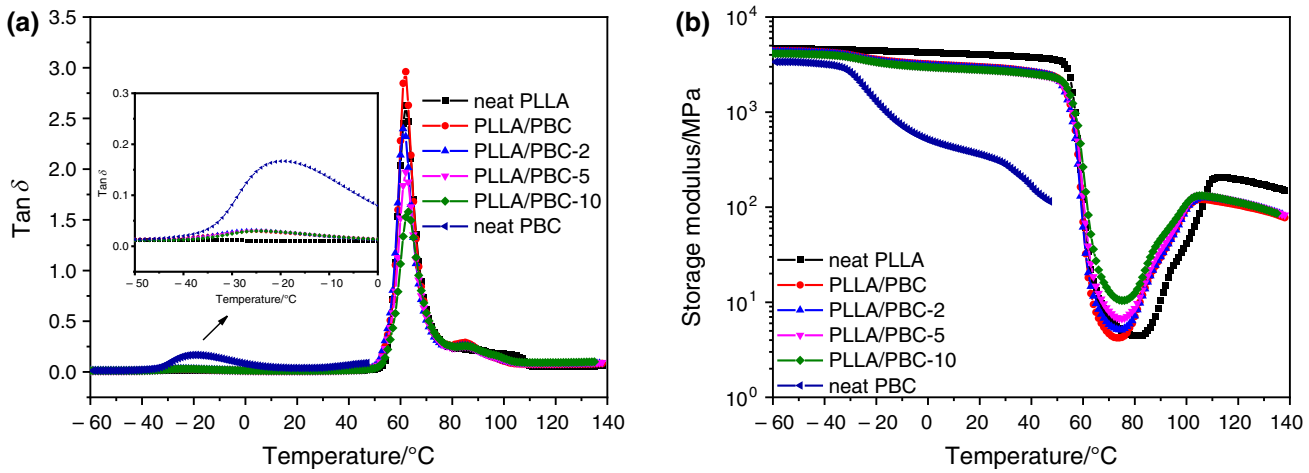

Fig. 12 DMA traces of neat components and their blends: **a** damping factor (tan δ) versus temperature and **b** storage modulus (E') versus temperature

The E' curves of neat components and their blends are shown in Fig. 12b. The E' of neat PBC dropped pronouncedly at about − 20 °C owing to the glass transition. The E' of neat PLLA declined pronouncedly at around 60 °C and rose markedly at approximately 90 °C due to its glass transition and cold crystallization behavior, respectively. For blends, when the temperature exceeded 74 °C, an increase in E' arising from the cold crystallization of PLLA could be observed. Neat PLLA and its blends displayed similar E' at temperatures below T_g of PBC due to the glassy state of PBC and PLLA. At temperatures between the T_g of PBC and PLLA or exceeding the T_{cc} of PLLA, blends showed lower E' than neat PLLA. This observation was due to PBC being in a rubbery or fluid state (the melting temperature of neat PBC was approximately 57.5 °C as determined by DSC, shown in Fig. S1), which reduced the interaction between segments and chains within the crystalline region of the PLLA. When the temperature ranged from T_g to T_{cc} of PLLA, the lowest E' value of 4.45 MPa was observed in neat PLLA. With PDLA concentration in blends changing

from 0 to 10 mass%, the lowest E' value in blends increased from 4.3 MPa for PLLA/PBC binary blend to 5.1 MPa for PLLA/PBC-2, 6.8 MPa for PLLA/PBC-5, and 10.4 MPa for PLLA/PBC-10, respectively. The improvement of E' might be attributed to the strengthened effect of SC-PLA crystals with high modulus on the PLLA matrix. In addition, the role of SC-PLA crystals as physical crosslinks restricted the motion of PLLA chains, consequently restraining the chain relaxation of PLLA.

Mechanical properties

Matrix crystallinity (X_m) can significantly influence the mechanical properties of PLLA-based blends. Therefore, the X_ms of melt-quenched tensile test bars were determined by analyzing the DSC curves shown in Fig. 1b. The results of the analysis are summarized in Table S1. There was a similar low homocrystallinity ($X_{c,\,HC}$) for neat PLLA and its blends. However, the stereocomplex crystallinity ($X_{c,\,SC}$) of PLLA/PBC/PDLA ternary blends increased as PDLA concentration increased, which led to an increase in X_m. From Table S1, The X_m of neat PLLA and PLLA/PBC binary blend was 4.9 and 5.4%, respectively. As PDLA concentration increased, the X_m values of the ternary blends increased to 7.9, 11.7, and 18.0% for PLLA/PBC-2, PLLA/PBC-5, and PLLA/PBC-10, respectively.

The stress–strain curves of neat PLLA and its blends are described in Fig. 13, and Table 3 presents the data on tensile properties. Neat PLLA exhibited a brittle fracture behavior, while the blends with or without PDLA exhibited ductile characteristics with distinct yield and stable neck growth. Rigid PLLA had Young's modulus of 2056 MPa, yield strength of 68.5 MPa, and elongation at break of 5.2%. Incorporating PBC into PLLA significantly increased elongation at break to 309.4% while decreasing yield strength, Young's modulus, and breaking strength to 49.8 MPa, 1483 MPa, and 39.9 MPa, respectively. Lower elongation at break and breaking strength were observed in the ternary blends, and compared to the binary blend, elongation at break of ternary blends decreased with increasing PDLA concentration. However, the elongation at break of PLLA/PBC-10 remained above 90%.

The phase morphology, as well as the crystalline and amorphous fractions, had a significant impact on the tensile properties of immiscible polymer blends. The PLLA/PBC binary blend with low X_m exhibited excellent toughness on account of the introduction of soft PBC, which is in line with previous reports [22]. The soft PBC phase acted as a stress concentrator when the PLLA/PBC blend was subjected to a load. The stress concentration might cause debonding at the interface between the matrix and the dispersed phase, resulting in the plastic deformation of the matrix. The reduction of the elongation at break of the ternary blends was primarily

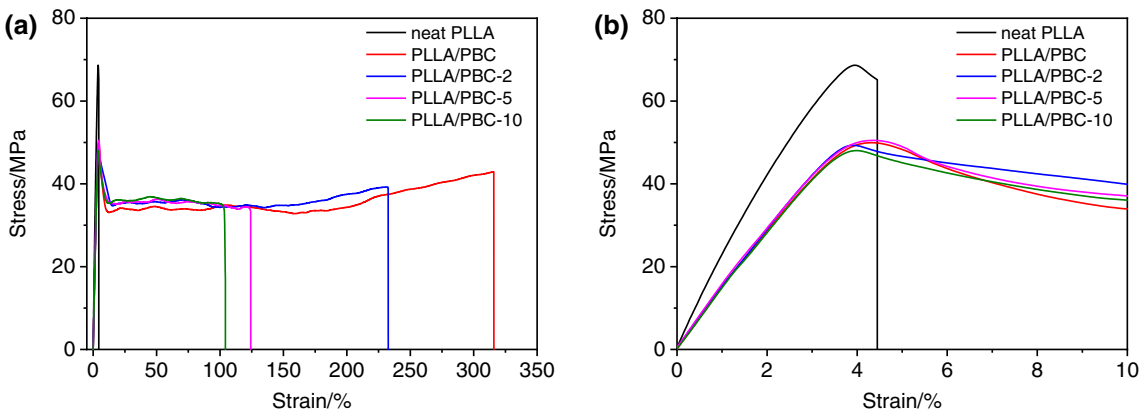

Fig. 13 **a** Tensile stress–strain curves of neat PLLA and its blends; **b** details of stress–strain curves at low strain

Table 3 Tensile properties parameters for neat PLLA and its blends

Sample	Young's modulus/MPa	Yield strength/MPa	Breaking strength/MPa	Elongation at break/%
Neat PLLA	2056 ± 29	68.5 ± 0.3	68.5 ± 0.3	5.2 ± 0.4
PLLA/PBC	1483 ± 23	49.8 ± 0.8	39.9 ± 2.3	309.4 ± 16.8
PLLA/PBC-2	1521 ± 28	48.8 ± 0.7	39.3 ± 1.4	247.2 ± 18.1
PLLA/PBC-5	1488 ± 28	50.2 ± 1.0	34.7 ± 1.0	136.8 ± 9.1
PLLA/PBC-10	1512 ± 56	47.7 ± 1.6	35.6 ± 1.0	97.2 ± 9.7

attributed to the increase in X_m. From Table S1, the formation of SC-PLA crystals increased the X_m of blends. The crystalline fractions were dense structures, resulting in a restrictive effect on polymer movement and thus reducing its extensibility [56]. Small amounts of SC-PLA crystals were formed after adding 2 mass% PDLA to the binary blend. At this point, the PLLA matrix formed a continuous amorphous phase with a discontinuous SC-PLA crystals region, resulting in a slight reduction in the elongation at break of the ternary blends. However, when PDLA concentration reached 5 mass% or higher, a continuous region composed of SC-PLA crystals was dispersed in the PLLA matrix, as determined by rheological results. The existence of the SC-PLA crystal network could significantly restrict molecular motion, which suppressed matrix plastic deformation caused by interfacial debonding during the stretching process. Therefore, the formation of the SC-PLA crystal network structure led to a marked drop of elongation at break for ternary blends. Furthermore, as determined by SEM results, the introduction of SC-PLA crystals increased the PBC domain size. The larger dispersed phase domain size could cause the blends to debond easily at a lower load, thereby reducing elongation at break and breaking strength of ternary blends. However, the PLLA/PBC-10 sample still exhibited higher elongation at break than the neat PLLA. This phenomenon suggested that the toughening effect of PBC on PLLA was retained after the addition of PDLA.

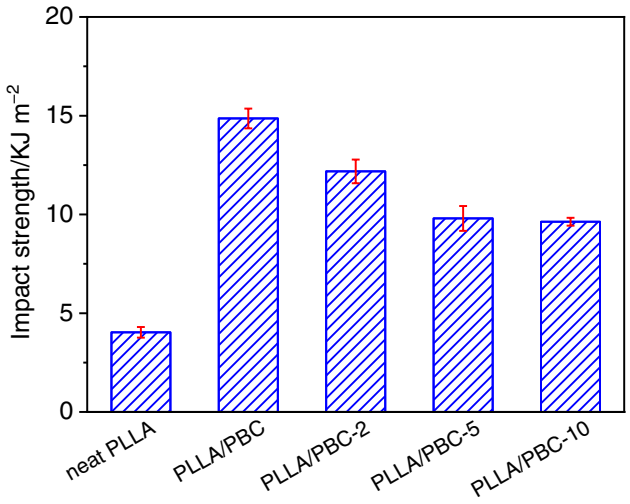

Fig. 14 Notched Izod impact strength for neat PLLA and its blends

Figure 14 presents the notched Izod impact strength of neat PLLA, PLLA/PBC binary, and PLLA/PBC/PDLA ternary blends at room temperature. Since the impact testing bars underwent the same thermal history as the tensile testing bars, their X_ms were similar. The addition of PBC significantly enhanced the impact toughness of PLLA. The impact strength increased from 4.0 kJ m^{-2} for neat PLLA to 14.9 kJ m^{-2} for the binary blend. After adding PDLA into the binary blend, the impact strength decreased with increasing PDLA concentration.

The SEM images of the impact-fractured surfaces for all samples are shown in Fig. 15. Neat PLLA had a relatively

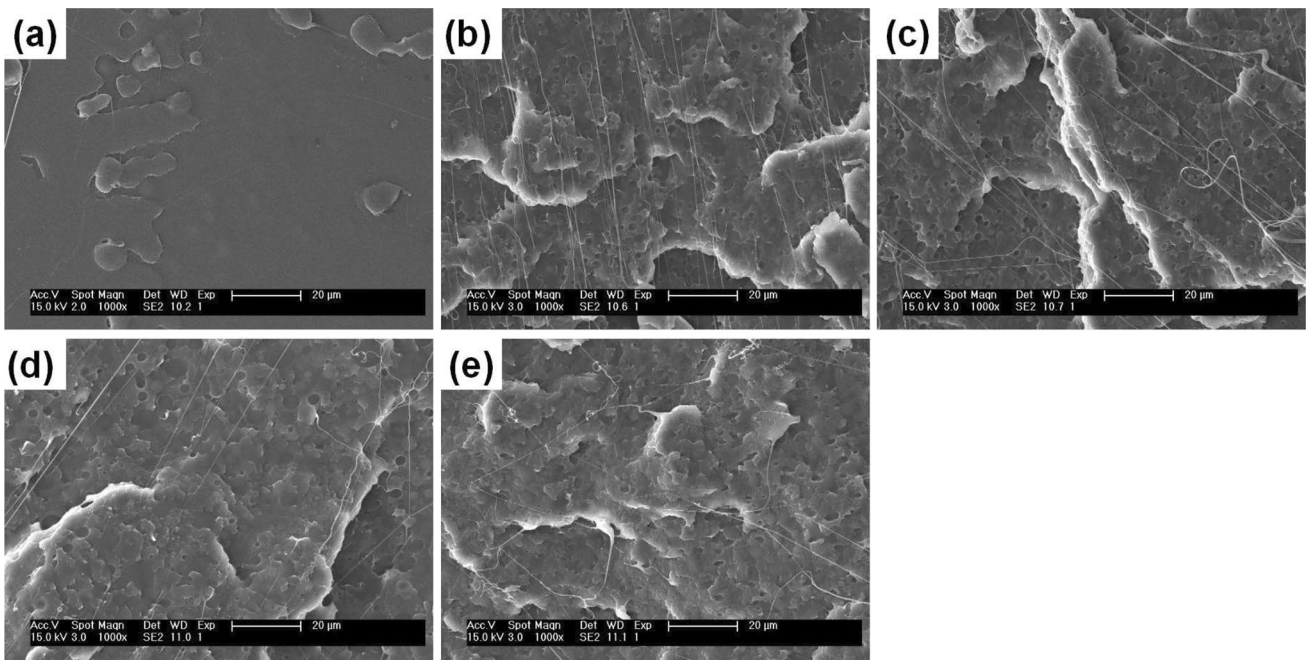

Fig. 15 SEM micrographs of the impact-fractured surfaces of neat PLLA and its blends: **a** neat PLLA; **b** PLLA/PBC; **c** PLLA/PBC-2; **d** PLLA/PBC-5; and **e** PLLA/PBC-10

smooth and flat surface, indicative of a classic brittle fracture. Compared to neat PLLA, all blends exhibited more rough and uneven fracture surfaces and evidence of ductile fractures such as cavitation, stress-whitening zones, and many long fibrils. When the toughed polymer was subjected to a load, crazing, cavitation, shear yielding, crack bridging, and shear banding were crucial processes for energy dissipation. Notably, as the PDLA concentration increased, the length of the fibrils dispersed on the impact-fractured surface of blends became shorter, and the number of fibrils decreased, indicating that plastic deformation of the matrix was suppressed due to the formation of SC-PLA crystals that increased X_m. As a result, the energy dissipation induced by matrix plastic deformation was decreased, thus reducing the impact strength of ternary blends.

Conclusions

In this study, fully biodegradable PLLA/PBC/PDLA ternary blends were prepared by melt blending at a low temperature of 180 °C. During the melt mixing process, PDLA and PLLA co-crystallized to form SC-PLA crystals, which exhibited high modulus and acted as physical crosslinks, significantly improving the melt viscosity and strength of the blends. When the concentration of PDLA reached 5 mass%, SC-PLA crystals formed a percolating network structure, resulting in a transition of the rheological behavior of the blend melts from liquid-like to solid-like. All blends displayed a phase separation morphology, and PBC domain size increased as the concentration of PDLA increased. SC-PLA crystals exhibited an excellent nucleation effect, significantly accelerating the crystallization process and increasing the X_c of the PLLA in the ternary blends. The PLLA/PBC/PDLA ternary blends with 5 mass% PDLA exhibited the highest X_c among all samples with a value of 47.0%. The introduction of SC-PLA crystals increased the elastic storage modulus of the PLLA/PBC blends while having little impact on the miscibility between PLLA and PBC. The elongation at break and impact strength of the blends decreased as PDLA concentration increased, but the blends retained high toughness. Notably, with the addition of 2 mass% PDLA, the ternary blends exhibited excellent balanced properties with an elongation at break of 247%, impact strength of 12.2 kJ m^{-2}, accelerated crystallization rate, and improved rheological behavior. These results demonstrate promising potential for sustainable PLLA-based materials with well-balanced properties.

Supplementary Information The online version contains supplementary material available at https://doi.org/10.1007/s10973-024-13245-x.

Acknowledgements This work was supported by the Science and Technology Department of Jilin Province (20230402067GH).

Author contributions Hongda Cheng contributed to conceptualization, methodology, data curation, writing—original draft, visualization, resources, methodology, and software. Mengdie Yu contributed to data curation, software, formal analysis, and conceptualization. Ye Zhang and Yanchun Yu contributed to software, data curation, and formal analysis. Hechang Shi contributed to data curation and software. Lijuan Wang contributed to conceptualization, resources, writing—reviewing and editing, investigation, and funding acquisition. Changyu Han contributed to conceptualization, resources, writing—reviewing and editing, investigation, and supervision. All authors discussed the results and contributed to the final manuscript; all authors read and approved the final manuscript.

Declarations

Conflict of interest The authors declare that they have no conflicts of interest/competing interests.

References

1. Zhou ZY, LaPointe AM, Shaffer TD, Coates GW. Nature-inspired methylated polyhydroxybutyrates from C1 and C4 feedstocks. Nat Chem. 2023;15(6):856–61. https://doi.org/10.1038/s41557-023-01187-0.
2. Castro-Aguirre E, Iñiguez-Franco F, Samsudin H, Fang X, Auras R. Poly(lactic acid)-mass production, processing, industrial applications, and end of life. Adv Drug Deliv Rev. 2016;107:333–66. https://doi.org/10.1016/j.addr.2016.03.010.
3. Nofar M, Sacligil D, Carreau PJ, Kamal MR, Heuzey MC. Poly (lactic acid) blends: processing, properties and applications. Int J Biol Macromol. 2019;125:307–60. https://doi.org/10.1016/j.ijbiomac.2018.12.002.
4. Hamad K, Kaseem M, Yang HW, Deri F, Ko YG. Properties and medical applications of polylactic acid: a review. Express Polym Lett. 2015;9(5):435–55. https://doi.org/10.3144/expresspolymlett.2015.42.
5. Yi L, Luo S, Cui L, Budai-Szűcs M, Móczó J, Pukánszky B. Processes taking place during the preparation and use of electrospun PLA fibers and their effect on controlled drug release. J Therm Anal Calorim. 2022;147(23):13191–9. https://doi.org/10.1007/s10973-022-11554-7.
6. Nofar M, Park CB. Poly (lactic acid) foaming. Prog Polym Sci. 2014;39(10):1721–41. https://doi.org/10.1016/j.progpolymsci.2014.04.001.
7. Menossi M, Salcedo F, Rivilli N, Nicolini AT, Alvarez VA, Ludueña LN. Biodegradable mulch films based on starch/poly (lactic acid)/poly (ε-caprolactone) ternary blends. J Polym Environ. 2023;31:2114–37. https://doi.org/10.1007/s10924-022-02721-w.
8. Terroba-Delicado E, Fiori S, Gomez-Caturla J, Montanes N, Sanchez-Nacher L, Torres-Giner S. Valorization of liquor waste derived spent coffee grains for the development of injection-molded polylactide pieces of interest as disposable food packaging and serving materials. Foods. 2022;11(8):1162. https://doi.org/10.3390/foods11081162.
9. Moldovan A, Cuc S, Prodan D, Rusu M, Popa D, Taut AC, Petean I, Bombos D, Doukeh R, Nemes O. Development and characterization of polylactic acid (PLA)-based nanocomposites used for food packaging. Polymers. 2023;15(13):2885. https://doi.org/10.3390/polym15132855.

10. Tümer EH, Erbil HY. Extrusion-based 3D printing applications of PLA composites: a review. Coatings. 2021;11(4):309. https://doi.org/10.3390/coatings11040390.
11. Huang WJ, Zhang XZ, Zheng X, Zhang Z, Ding BA, Zhang Y, Wang XH. Synergistic enhancement of modified sericite on rheological and foaming properties of poly (lactic acid). Int J Biol Macromol. 2023;253: 127235. https://doi.org/10.1016/j.ijbiomac.2023.127235.
12. Li ZK, Song SX, Lv X, Sun SL. Enhanced the melt strength, toughness and stiffness balance of the reactive PB-g-SAG core–shell particles modified polylactide blends with the aid of a multifunctional epoxy-based chain extender. J Polym Res. 2021;28(5):151. https://doi.org/10.1007/s10965-021-02511-3.
13. Zhou YH, Lei L, Yang B, Li JB, Ren J. Preparation and characterization of polylactic acid (PLA) carbon nanotube nanocomposites. Polym Test. 2018;68:34–8. https://doi.org/10.1016/j.polymertesting.2018.03.044.
14. Saeidlou S, Huneault MA, Li HB, Park CB. Poly(lactic acid) crystallization. Prog Polym Sci. 2012;37(12):1657–77. https://doi.org/10.1016/j.progpolymsci.2012.07.005.
15. Wang SY, Jiang C, Xie HH, Zeng JB, Li YD. Compatibilization of polylactide/poly(butylene adipate-co-terephthalate) blends with epoxidized natural rubber as a reactive compatibilizer. Ind Crop Prod. 2023;205: 117447. https://doi.org/10.1016/j.indcrop.2023.117447.
16. Zhao XP, Yu JJ, Wang X, Huang ZP, Zhou WY, Peng SX. Strong synergistic toughening and compatibilization enhancement of carbon nanotubes and multi-functional epoxy compatibilizer in high toughened polylactic acid (PLA)/poly (butylene adipate-co-terephthalate) (PBAT) blends. Int J Biol Macromol. 2023;250: 126204. https://doi.org/10.1016/j.ijbiomac.2023.126204.
17. Fernández-Tena A, Otaegi I, Irusta L, Sebastián V, Guerrica-Echevarria G, Müller AJ, Aranburu N. High-impact PLA in compatibilized PLA/PCL blends: optimization of blend composition and type and content of compatibilizer. Macromol Mater Eng. 2023;308(12):2300213. https://doi.org/10.1002/mame.202300213.
18. Aliotta L, Gigante V, Geerinck R, Coltelli MB, Lazzeri A. Micromechanical analysis and fracture mechanics of poly(lactic acid) (PLA)/polycaprolactone (PCL) binary blends. Polym Test. 2023;121: 107984. https://doi.org/10.1016/j.polymertesting.2023.107984.
19. Ge QY, Dou Q. Preparation of supertough polylactide/polybutylene succinate/epoxidized soybean oil bio-blends by chain extension. ACS Sustain Chem Eng. 2023;11(26):9620–9. https://doi.org/10.1021/acssuschemeng.3c01042.
20. Zhang XZ, Zhang Y. Reinforcement effect of poly(butylene succinate) (PBS)-grafted cellulose nanocrystal on toughened PBS/polylactic acid blends. Carbohydr Polym. 2016;140:374–82. https://doi.org/10.1016/j.carbpol.2015.12.073.
21. Loureiro NC, Esteves JL, Viana JC, Ghosh S. Mechanical characterization of polyhydroxyalkanoate and poly(lactic acid) blends. J Thermoplast Compos Mater. 2015;28(2):195–213. https://doi.org/10.1177/0892705712475020.
22. Wang XM, Zhuang YG, Dong LS. Study of biodegradable polylactide/poly(butylene carbonate) blend. J Appl Polym Sci. 2013;127(1):471–7. https://doi.org/10.1002/app.37735.
23. Wang XM, Zhuang YG, Dong LS. Properties of biodegradable poly(butylene carbonate) (PBC) composites with fumed silica nanoparticles. J Therm Anal Calorim. 2013;114(1):77–84. https://doi.org/10.1007/s10973-012-2862-9.
24. Ge F, Wang XM, Ran XH. Effect of annealing on the properties of polylactide/poly(butylene carbonate) blend. Adv Polym Technol. 2018;37(5):1335–44. https://doi.org/10.1002/adv.21792.
25. Refaa Z, Boutaous MH, Xin SH, Siginer DA. Thermophysical analysis and modeling of the crystallization and melting behavior of PLA with talc. J Therm Anal Calorim. 2017;128(2):687–98. https://doi.org/10.1007/s10973-016-5961-1.
26. Zou GX, Zhang X, Zhao CX, Li JC. The crystalline and mechanical properties of PLA/layered silicate degradable composites. Polym Sci Ser A. 2012;54(5):393–400. https://doi.org/10.1134/S0965545X12050148.
27. Pan HW, Cao ZW, Chen YJ, Wang XY, Jia SL, Yang HL, Zhang HL, Dong LS. Effect of molecular stereoregularity on the transcrystallinization properties of poly(L-lactide)/basalt fiber composites. Int J Biol Macromol. 2019;137:238–46. https://doi.org/10.1016/j.ijbiomac.2019.06.147.
28. Pan HW, Wang XY, Jia SL, Lu ZF, Bian JJ, Yang HL, Han LJ, Zhang HL. Fiber-induced crystallization in polymer composites: a comparative study on poly(lactic acid) composites filled with basalt fiber and fiber powder. Int J Biol Macromol. 2021;183:45–54. https://doi.org/10.1016/j.ijbiomac.2021.04.104.
29. Guo S, Zhou Z, Yu SL, Chen ZB, Xiang HX, Zhu MF. The synergistic effect of heterogeneous nucleation and stress-induced crystallization on supramolecular structure and performances of poly(lactic acid) melt-spun fibers. Int J Biol Macromol. 2023;226:1579–87. https://doi.org/10.1016/j.ijbiomac.2022.11.270.
30. He DR, Wang YM, Shao CG, Zheng GQ, Li Q, Shen CY. Effect of phthalimide as an efficient nucleating agent on the crystallization kinetics of poly(lactic acid). Polym Test. 2013;32(6):1088–93. https://doi.org/10.1016/j.polymertesting.2013.06.005.
31. Schmidt SC, Hillmyer MA. Polylactide stereocomplex crystallites as nucleating agents for isotactic polylactide. J Polym Sci Pol Phys. 2001;39(3):300–13. https://doi.org/10.1002/1099-0488(20010201)39:3%3c300::AID-POLB1002%3e3.0.CO;2-M.
32. Anderson KS, Hillmyer MA. Melt preparation and nucleation efficiency of polylactide stereocomplex crystallites. Polymer. 2006;47(6):2030–5. https://doi.org/10.1016/j.polymer.2006.01.062.
33. Saeidlou S, Huneault MA, Li H, Park CB. Poly(lactic acid) stereocomplex formation: application to PLA rheological property modification. J Appl Polym Sci. 2014;131(22):41073. https://doi.org/10.1002/app.41073.
34. Yan C, Hou DF, Zhang K, Yang MB. Effects of PDLA molecular weight on the crystallization behaviors and rheological properties of asymmetric PDLA/PLLA blends. Polymer. 2023;270: 125764. https://doi.org/10.1016/j.polymer.2023.125764.
35. Park HS, Hong CK. Relationship between the stereocomplex crystallization behavior and mechanical properties of PLLA/PDLA blends. Polymers. 2021;13(11):1851. https://doi.org/10.3390/polym13111851.
36. Su XL, Feng LH, Yu DM. Formation of stereocomplex crystal and its effect on the morphology and property of PDLA/PLLA blends. Polymers. 2020;12(11):2515. https://doi.org/10.3390/polym12112515.
37. Frone AN, Baciu DD, Popa MS, Nicolae CA, Gabor AR, Raduly MF, Fierascu RC, Panaitescu DM. Thermal behavior and thermomechanical properties of biocompatible poly(lactic acid)/allyl-POSS nanohybrids. J Therm Anal Calorim. 2023;148(20):10465–79. https://doi.org/10.1007/s10973-023-12196-z.
38. Boruvka M, Behalek L, Lenfeld P, Brdlik P, Habr J, Wongmanee S, Bobek J, Pechociakova M. Solid and microcellular polylactide nucleated with PLA stereocomplex and cellulose nanocrystals. J Therm Anal Calorim. 2020;142(2):695–713. https://doi.org/10.1007/s10973-020-09477-2.
39. Sun JR, Yu HY, Zhuang XL, Chen XS, Jing XB. Crystallization behavior of asymmetric PLLA/PDLA blends. J Phys Chem B. 2011;115(12):2864–9. https://doi.org/10.1021/jp111894m.
40. Tsuji H. Poly(lactide) stereocomplexes: formation, structure, properties, degradation, and applications. Macromol Biosci. 2005;5(7):569–97. https://doi.org/10.1002/mabi.200500062.

41. Wu DF, Wu L, Zhang M, Zhao YL. Viscoelasticity and thermal stability of polylactide composites with various functionalized carbon nanotubes. Polym Degrad Stab. 2008;93(8):1577–84. https://doi.org/10.1016/j.polymdegradstab.2008.05.001.
42. Sabzi M, Jiang L, Liu F, Ghasemi I, Atai M. Graphene nanoplatelets as poly(lactic acid) modifier: linear rheological behavior and electrical conductivity. J Mater Chem A. 2013;1(28):8253–61. https://doi.org/10.1039/c3ta11021d.
43. Bärwinkel S, Seidel A, Hobeika S, Hufen R, Mörl M, Altstädt V. Morphology formation in PC/ABS blends during thermal processing and the effect of the viscosity ratio of blend partners. Materials. 2016;9(8):659. https://doi.org/10.3390/ma9080659.
44. Everaert V, Aerts L, Groeninckx G. Phase morphology development in immiscible PP/(PS/PPE) blends influence of the melt-viscosity ratio and blend composition. Polymer. 1999;40(24):6627–44. https://doi.org/10.1016/S0032-3861(99)00048-8.
45. Huang HX. Macro, micro and nanostructured morphologies of multiphase polymer systems. In: Boudenne A, Ibos L, Candau Y, Thomas S, editors. Handbook of multiphase polymer systems. New Jersey: Wiley; 2011. p. 161–249.
46. Wu X, Liu YX, Wu HP, Wu H, Wang HJ, Duan YX, Zhang JM. Cellulose nanocrystals-mediated phase morphology of PLLA/TPU blends for 3D printing. Chin J Polym Sci. 2022;40(3):299–309. https://doi.org/10.1007/s10118-022-2665-9.
47. Vainio TP, Seppala JV. The effect of mixer type and processing conditions on the morphology of polyamide/polypropylene blend. Polym Polym Compos. 1993;1(6):427–37. https://doi.org/10.1177/096739119300100604.
48. Sakai F, Nishikawa K, Inoue Y, Yazawa K. Nucleation enhancement effect in poly(L-lactide) (PLLA)/poly(ε-caprolactone) (PCL) blend induced by locally activated chain mobility resulting from limited miscibility. Macromolecules. 2009;42(21):8335–42. https://doi.org/10.1021/ma901547a.
49. He Y, Fan ZY, Hu YF, Wu T, Jia W, Li SM. DSC analysis of isothermal melt-crystallization, glass transition and melting behavior of poly(L-lactide) with different molecular weights. Eur Polym J. 2007;43(10):4431–9. https://doi.org/10.1016/j.eurpolymj.2007.07.007.
50. Li JN, Qiu ZB. Effect of low loadings of cellulose nanocrystals on the significantly enhanced crystallization of biodegradable poly(butylene succinate-co-butylene adipate). Carbohydr Polym. 2019;205:211–6. https://doi.org/10.1016/j.carbpol.2018.10.035.
51. Avrami M. Kinetics of phase change. I general theory. J Chem Phys. 1939;7(12):1103–12. https://doi.org/10.1063/1.1750380.
52. Avrami M. Kinetics of phase change. II transformation-time relations for random distribution of nuclei. J Chem Phys. 1940;8(2):212–24. https://doi.org/10.1063/1.1750631.
53. Tsuji H, Takai H, Saha SK. Isothermal and non-isothermal crystallization behavior of poly(L-lactic acid): effects of stereocomplex as nucleating agent. Polymer. 2006;47(11):3826–37. https://doi.org/10.1016/j.polymer.2006.03.074.
54. Liang R, Chen YC, Zhang CQ, Yin J, Liu XL, Wang LK, Kong R, Feng X, Yang JJ. Crystallization behavior of biodegradable poly(ethylene adipate) modulated by a benign nucleating agent: zinc phenylphosphonate. Chin J Polym Sci. 2017;35(4):558–68. https://doi.org/10.1007/s10118-017-1917-6.
55. Xu ZH, Niu YH, Yang L, Xie WY, Li H, Gan ZH, Wang ZG. Morphology, rheology and crystallization behavior of polylactide composites prepared through addition of five-armed star polylactide grafted multiwalled carbon nanotubes. Polymer. 2010;51(3):730–7. https://doi.org/10.1016/j.polymer.2009.12.017.
56. Harnkarnsujarit N, Li Y. Structure-property modification of microcrystalline cellulose film using agar and propylene glycol alginate. J Appl Polym Sci. 2017;134(47):45533. https://doi.org/10.1002/app.45533.